OCEAN ACIDIFICATION

Climate change drives rapid decadal acidification in the Arctic Ocean from 1994 to 2020

Di Qi[1,2,3], Zhangxian Ouyang[4], Liqi Chen[1,2]*, Yingxu Wu[1], Ruibo Lei[5], Baoshan Chen[4], Richard A. Feely[6], Leif G. Anderson[7], Wenli Zhong[8], Hongmei Lin[2], Alexander Polukhin[9], Yixing Zhang[2], Yongli Zhang[10], Haibo Bi[3,11], Xinyu Lin[2], Yiming Luo[12], Yanpei Zhuang[1], Jianfeng He[5], Jianfang Chen[13], Wei-Jun Cai[4]*

The Arctic Ocean has experienced rapid warming and sea ice loss in recent decades, becoming the first open-ocean basin to experience widespread aragonite undersaturation [saturation state of aragonite (Ω_{arag}) < 1]. However, its trend toward long-term ocean acidification and the underlying mechanisms remain undocumented. Here, we report rapid acidification there, with rates three to four times higher than in other ocean basins, and attribute it to changing sea ice coverage on a decadal time scale. Sea ice melt exposes seawater to the atmosphere and promotes rapid uptake of atmospheric carbon dioxide, lowering its alkalinity and buffer capacity and thus leading to sharp declines in pH and Ω_{arag}. We predict a further decrease in pH, particularly at higher latitudes where sea ice retreat is active, whereas Arctic warming may counteract decreases in Ω_{arag} in the future.

In the global ocean, an increase in anthropogenic carbon dioxide (CO_2) has led to decreases in seawater pH based on the total hydrogen ion concentration scale (pH_T) and the saturation state of the calcium carbonate mineral aragonite (Ω_{arag}) in a process known as ocean acidification (*1*). Although substantial regional and decadal variability in ocean acidification, driven by climate-induced atmospheric and oceanic circulation changes, has been observed in low- and mid-latitude ocean basins (*2*–*4*) and in the Southern Ocean (*3*), long-term ocean acidification rates generally have followed the trends predicted from the increase in the concentration of CO_2 in the atmosphere (*2*, *3*). For the Arctic Ocean, although numerical models have predicted high acidification rates (*5*–*8*), observation-based decadal rates of surface water pH_T and Ω_{arag} change are sparse. Over the past three decades, climate warming has induced notable changes in the Arctic atmosphere-ice-ocean system (fig. S1). These changes include (i) a rapid sea ice retreat from a nearly fully ice-covered state before the 1990s to an ice-free state in the southern part of the Canada Basin and a partially ice-covered state in the northern part of the basin (*9*), (ii) a change from cyclonic circulation in the 1990s to an anomalous anticyclonic circulation pattern (*10*), and (iii) a spin-up of the Beaufort Gyre (*11*) over the past 20 years (fig. S1). There are also increases in freshwater storage (*11*), Pacific Summer Water inflow (*12*), biological production (*13*), stratification (*14*), air-sea CO_2 exchanges and carbon sinks (*15*, *16*), and nutricline depth (*17*) and decreases in surface nutrients (*18*) and subsurface anthropogenic CO_2 storage (*19*). In addition, pH_T and calcium carbonate saturation conditions have been substantially altered by these changes (*20*–*26*). For example, the Canada Basin was the first open-ocean basin where surface aragonite undersaturation (i.e., Ω_{arag} < 1) was detected (*20*, *22*) together with subsurface (*21*, *27*) and intermediate water (*28*, *29*) acidification. Thus, the Arctic Ocean is considered to be a bellwether of global climate change and ocean acidification (*30*).

Here, by using pH_T and Ω_{arag} estimates derived from data collected on 47 Arctic research cruises from 1994 to 2020 (see materials and methods), we document the high rates of long-term ocean acidification trends and basin-scale spatial expansion in terms of both pH_T and Ω_{arag} declines in the western Arctic Ocean. With this dataset, we further examine how sea ice loss and increasing atmospheric CO_2 have altered the sea-surface carbonate chemistry over the past two decades, and we propose an "ice melt–driven enhanced anthropogenic CO_2 acidification" mechanism to explain such rapid rates of regional ocean acidification.

The pH_T and Ω_{arag} values were calculated based on underway measurements of the partial pressure of CO_2 (P_{CO_2}) and salinity-derived total alkalinity (TA), together with sea surface temperature and salinity, from 1994 to 2020 (table S1). Data were supplemented with pH_T and Ω_{arag}, which were calculated from discrete measurements of TA and dissolved inorganic carbon (DIC) (see materials and methods). The salinity-derived TA and corresponding calculated DIC values match well with those of the discrete samples, yielding uncertainties of less than ±14 μmol kg^{-1} (fig. S2), which are further quality controlled as described in the materials and methods. The combined uncertainties of estimated pH_T and Ω_{arag} were 0.0113 and 0.0109, respectively, which were computed using the uncertainty propagation routine for CO2SYS (*31*).

Our results show that the area of sea surface with relatively low pH_T (<8.05) and Ω_{arag} (<1) expanded substantially (~0 to 0.88 × 10^6 km^2) from 1994 to 2020, not only increasing in areal coverage but also extending into higher latitudes in the western Arctic Ocean (Fig. 1). During the 1990s, more than 90% of the western Arctic Ocean basin waters were covered by sea ice, with a high pH_T (8.17 ± 0.05), and were supersaturated with respect to aragonite (Ω_{arag} = 1.46 ± 0.23) (Fig. 1, A and E). These initial conditions of the relatively higher pH_T and Ω_{arag} in the sea ice–covered period are due to the absence of gas exchange to replenish CO_2 from the atmosphere and low water temperature (i.e., for the same TA and DIC values, pH_T is higher in cold than warm waters). As sea ice in the western Arctic Ocean basin began to melt beyond the annual seasonal cycle of advance and retreat in the early 2000s, relatively lower pH_T (8.12 ± 0.04) and Ω_{arag} (1.21 ± 0.14) were observed in surface waters. This acidification happened first in the southern Canada Basin and slope and then extended northward to 76°N (Fig. 1, B and F). By the late 2000s, extreme summertime sea ice retreat mediated by both climate change and natural variability led to a broad ice-free area (~1.7 × 10^6 km^2) with a large-scale lower pH_T (8.04 ± 0.02) and aragonite undersaturation (Ω_{arag} = 0.97 ± 0.05) that extended into the central Canada Basin (Fig. 1, C and G). Whereas the pH_T decrease could be attributed to a combination of rapid warming and CO_2 uptake from the atmosphere, the Ω_{arag} decrease was mainly due to CO_2 uptake because warming would result in an opposite trend. From 2011 to 2020, although the overall sea ice concentration and pH_T and Ω_{arag} values were similar to those of the late 2000s, the areas of low-pH_T (8.02 ± 0.01) and Ω_{arag}-undersaturated (0.95 ± 0.05) waters continued to expand northwestward (Fig. 1, D and H). We attribute this acidification to the continuously increasing atmospheric CO_2 uptake over the expanded ice-free regions. Overall, from the 1990s to the 2010s, rapid sea ice loss and

[1]Polar and Marine Research Institute, College of Harbor and Coastal Engineering, Jimei University, Xiamen 361021, China. [2]Third Institute of Oceanography, Ministry of Natural Resources, Xiamen 361005, China. [3]Center for Ocean Mega-Science, Chinese Academy of Sciences, Qingdao 266071, China. [4]School of Marine Science and Policy, University of Delaware, Newark, DE, USA. [5]Key Laboratory for Polar Science of the Ministry of Natural Resources, Polar Research Institute of China, Shanghai 200136, China. [6]Pacific Marine Environmental Laboratory–National Oceanic and Atmospheric Administration, Seattle, WA, USA. [7]Department of Marine Sciences, University of Gothenburg, SE-412 96 Gothenburg, Sweden. [8]Key Laboratory of Physical Oceanography, Ocean University of China, Shandong, China. [9]P.P. Shirshov Institute of Oceanology, Russian Academy of Sciences, Moscow, Russia. [10]School of Marine Science and Technology, Tianjin University, Tianjin, China. [11]Key Laboratory of Marine Geology and Environment, Chinese Academy of Sciences, Qingdao 266071, China. [12]School of Marine Sciences, Sun Yat-Sen University, Zhuhai, China. [13]Second Institute of Oceanography, Ministry of Natural Resources, Hangzhou 310012, China.
*Corresponding author. Email: chenliqi@tio.org.cn (L.C.); wcai@udel.edu (W.-J.C.)

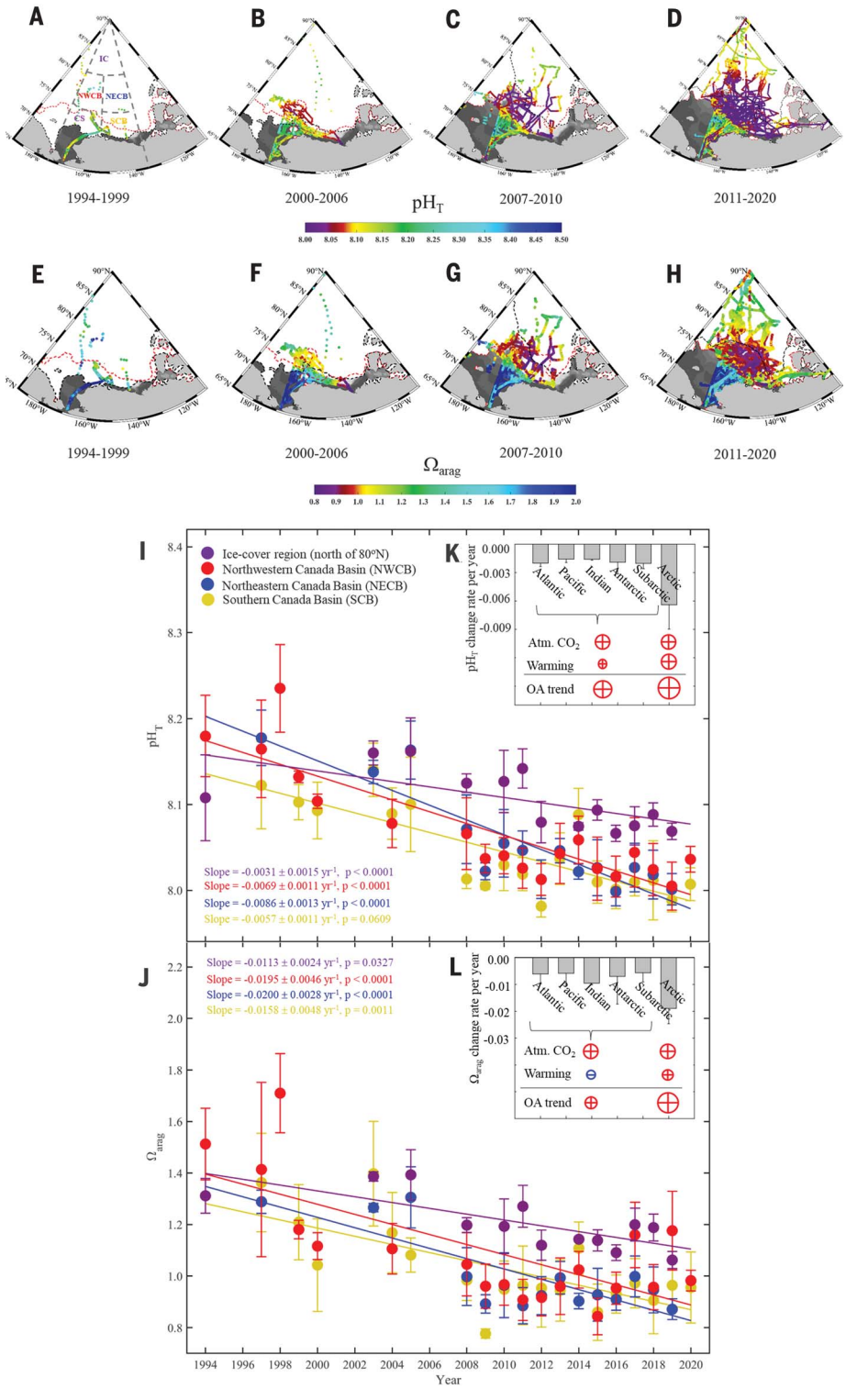

Fig. 1. Observations of ocean acidification and its decadal summertime trends in the western Arctic Ocean. (**A** to **H**) pH$_T$ [(A) to D)] and Ω_{arag} [(E) to (H)] in the western Arctic Ocean during 1994 to 1999, 2000 to 2006, 2007 to 2010, and 2011 to 2020. The black dashed lines show the ice edge (with an ice concentration threshold of 15% and gray shading representing sea ice concentration) during the first week of September during the first year of the subperiod; the red dashed lines show the location of that edge during the final year of the subperiod. Cruise information is provided in table S1. Sea ice edge data are from the National Snow and Ice Data Center (https://nsidc.org/data/seaice_index/). (**I** and **J**) decadal summertime trends of pH$_T$ and Ω_{arag}. Uncertainties associated with the trends were assessed by the Monte Carlo approach (see methods for detailed calculations). The error bars represent the combined uncertainty from sample measurements, carbonate system calculations, and the gridding-induced spatiotemporal variability. (**K** and **L**) Comparison of rates and mechanisms of acidification in the Arctic and other oceans. The gray vertical bars show annual rates, and the circles indicate the relative contributions of component mechanisms and their overall acidification effect. A red-plus circle indicates a positive contribution to acidification (or a positive net effect), and a blue-minus circle indicates an effect that counters acidification; the size of each circle indicates relative magnitude. The Arctic Ocean acidification rate was calculated as the average of the rates obtained in this study for the four western Arctic Ocean subregions (SCB, NECB, NWCB, and IC); decadal trend values for the other ocean basins were obtained from previous studies listed in table S2. Error bars represent the standard deviation of the mean rates. OA, ocean acidification.

acidification co-occurred in the western Arctic Ocean, but thereafter, relatively slow acidification occurred, accompanied by interannual fluctuation in sea ice coverage.

To quantify the long-term trends in pH$_T$ and Ω_{arag}, we first divided the western Arctic Ocean into five subregions based on spatial patterns of decadal ice retreat and ocean acidification expansion: the Chukchi Sea shelf (CS), Southern Canada Basin (SCB), Northeastern Canada Basin (NECB), Northwestern Canada Basin (NWCB), and permanent ice-covered region (IC, north of 80°N) (i.e., where minimal sea ice concentration is >70%) (Fig. 1A). We then averaged pH$_T$ and Ω_{arag} within each grid cell (0.1° latitude by 0.25° longitude) to obtain daily and monthly means for each cruise dataset. Finally, we averaged the gridded results within each subregion to obtain monthly and yearly (from June to October) means (see materials and methods).

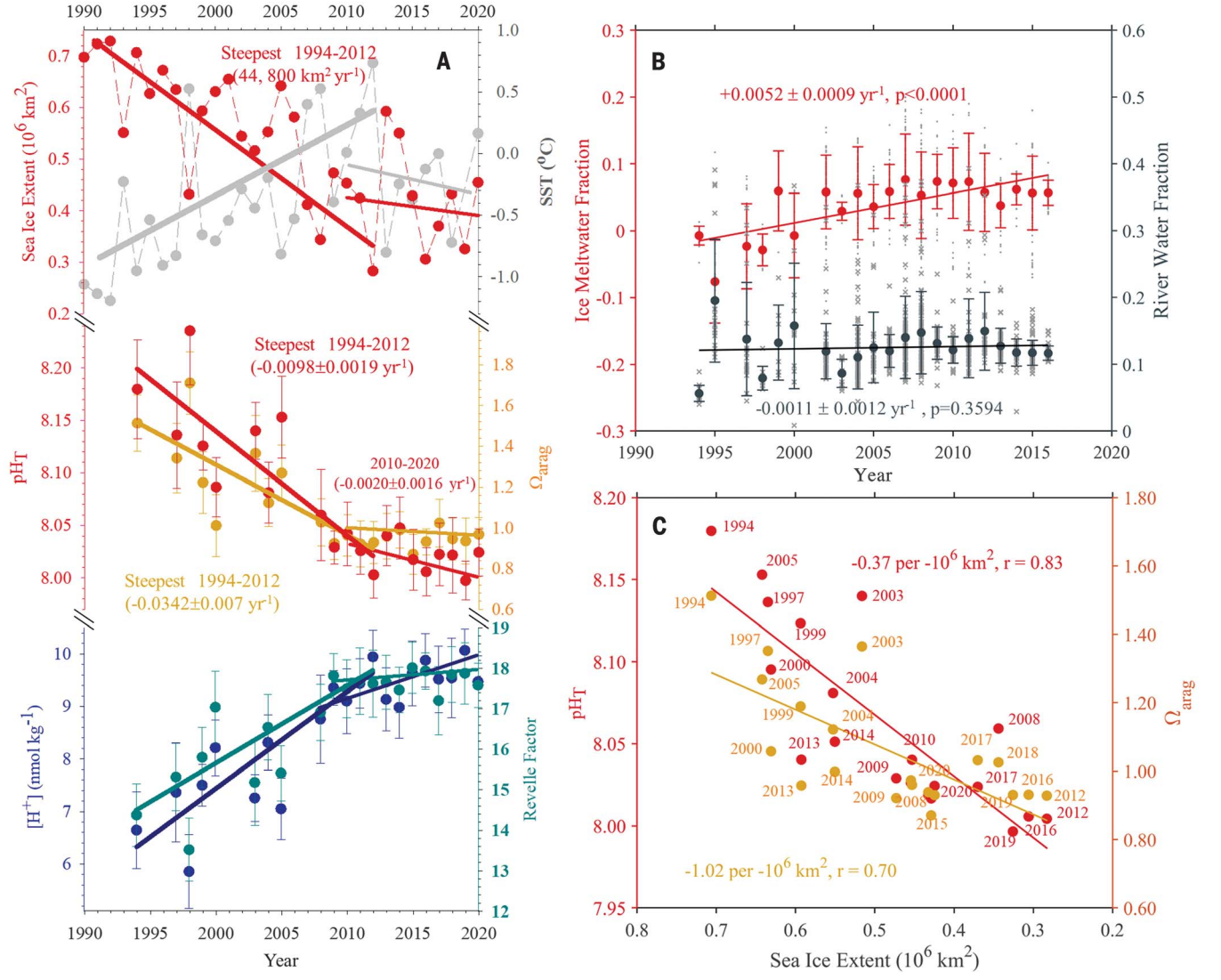

Fig. 2. Linking Arctic Ocean basin acidification to sea ice loss. (**A**) Sea ice loss, acidification status, and CO_2 buffer capacity (Revelle factor) in the rapid sea ice melt regions of the Canada Basin (including SCB, NECB, and NWCB). The Revelle factor (the ratio of $\partial PCO_2/PCO_2$ to $\partial DIC/DIC$) is a general measure of the ocean's sensitivity to an increase in CO_2. The sea surface temperature (SST) data were obtained from the Advanced Very High Resolution Radiometer (AVHRR) (*39*), whereas the sea ice extent data were obtained from the National Snow and Ice Data Center. Note that we use September monthly means to represent the decadal trends of sea ice extent. The middle and bottom panels show the mean decadal trends in the rapid ice melt area of the Canada Basin (south of 80°N), including the SCB, NECB, and NWCB regions. (**B**) Long-term change in fractions of meltwater and river water in the surface water (≤20 m) of the Canada Basin. The calculation methods follow those in (*20*, *21*). (**C**) Relationships between sea ice extent and pH_T and Ω_{arag}. The sea ice extent data are from https://nsidc.org/data/G02135/versions/3.

Different grid sizes, averaging schemes, deseasonalization treatments, and sensitivity tests (randomly removing 15 or 30% of measurements or cruises) were tested (figs. S3 to S11) for the determination of long-term trends. These various approaches yielded comparable and consistent rates of sea surface pH_T and Ω_{arag} decrease in all subregions except for the NWCB and CS, where undersampling in the former and the large natural spatiotemporal variability in the latter prohibit a good performance of deseasonalization.

Our results revealed rapid acidification in the western Arctic Ocean basins, with a mean annual rate of −0.0069 ± 0.0011 for pH_T and −0.0216 ± 0.0040 for Ω_{arag} from 1994 to 2020 (table S2). These rates are approximately four and three times faster, respectively, than the long-term decline rates in other ocean basins [Fig. 1, K and L, table S2, and (*32*)]. Similarly, the increase rate (0.128 ± 0.019 nmol kg^{-1} $year^{-1}$) of hydrogen ion [H^+] is also about four times faster than that in other ocean basins (table S2). The mean annual acidification rate was highest in the NECB (−0.0086 ± 0.0013 for pH_T and −0.020 ± 0.0028 for Ω_{arag}) and slowest in the ice-covered higher-latitude ocean basin (Fig. 1, I and J). These observational rates in the western Arctic basins are much faster than those projected by both regional and global models (e.g., −0.0025 to −0.0030 $year^{-1}$ for pH) (*5*–*8*). By contrast, we found a relatively slower rate of acidification on the CS than in the basins, with a mean annual rate of change of −0.0031 ± 0.0024 for pH_T and −0.0009 ± 0.0138 for Ω_{arag} (fig. S12).

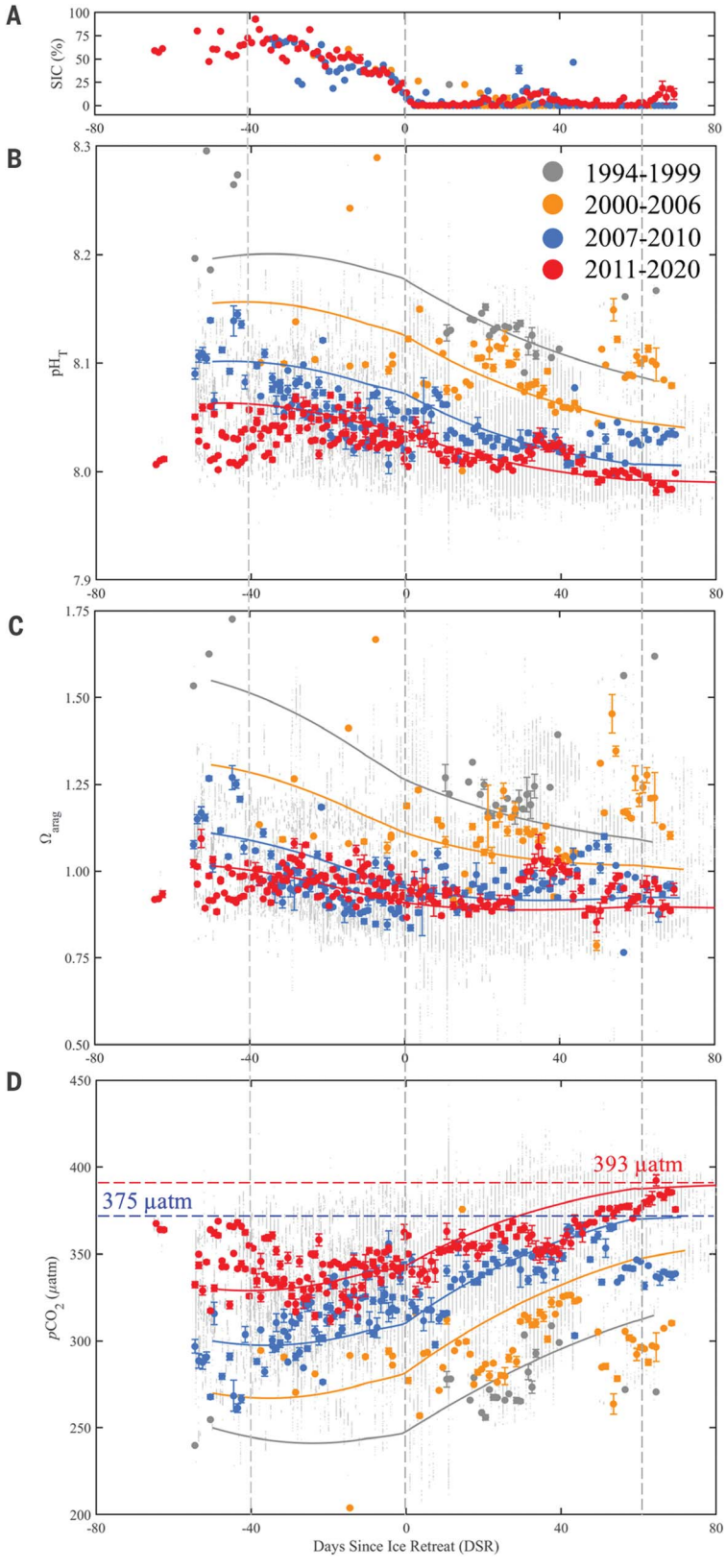

Fig. 3. Evolution of pH_T and Ω_{arag} as a function of days since ice retreat from 1994 to 2020 on the Arctic Ocean basin. (**A** to **D**) Sea ice concentration (SIC) (A), surface water pH_T (B), surface water Ω_{arag} (C), and surface water PCO_2 (D). The dots and error bars represent the means and standard deviations of SIC, pH_T, Ω_{arag}, and PCO_2 within 1 day's intervals. The "clouds" of gray dots in the background show individual data points. The solid lines show the 1D model–simulated days since ice retreat (DSR) dependences of these two CO_2 system parameters for four periods using a constant heating rate and panel until the DSR is 60, at which point the temperature is then held constant. The blue and red dashed lines represent the atmospheric CO_2 level in the 2007 to 2010 and 2011 to 2020 periods, respectively. See materials and methods for an explanation. The vertical dashed gray lines denote DSR of −40, 0, and 60 days.

The long-term acidification rates on the CS are likely mitigated by a strong and increasing biological CO_2 removal driven by nutrient inputs from the Pacific Ocean, which uses and counteracts CO_2 influx from the atmosphere (*13*, *16*, *33*).

When we focus on the regions of massive sea ice loss in the Canada Basin (including SCB, NWCB, and NECB), a notable finding appears—the decreases in pH_T and Ω_{arag} are strongly correlated with the decrease in sea ice extent over the past 26 years (Fig. 2). Notably, the

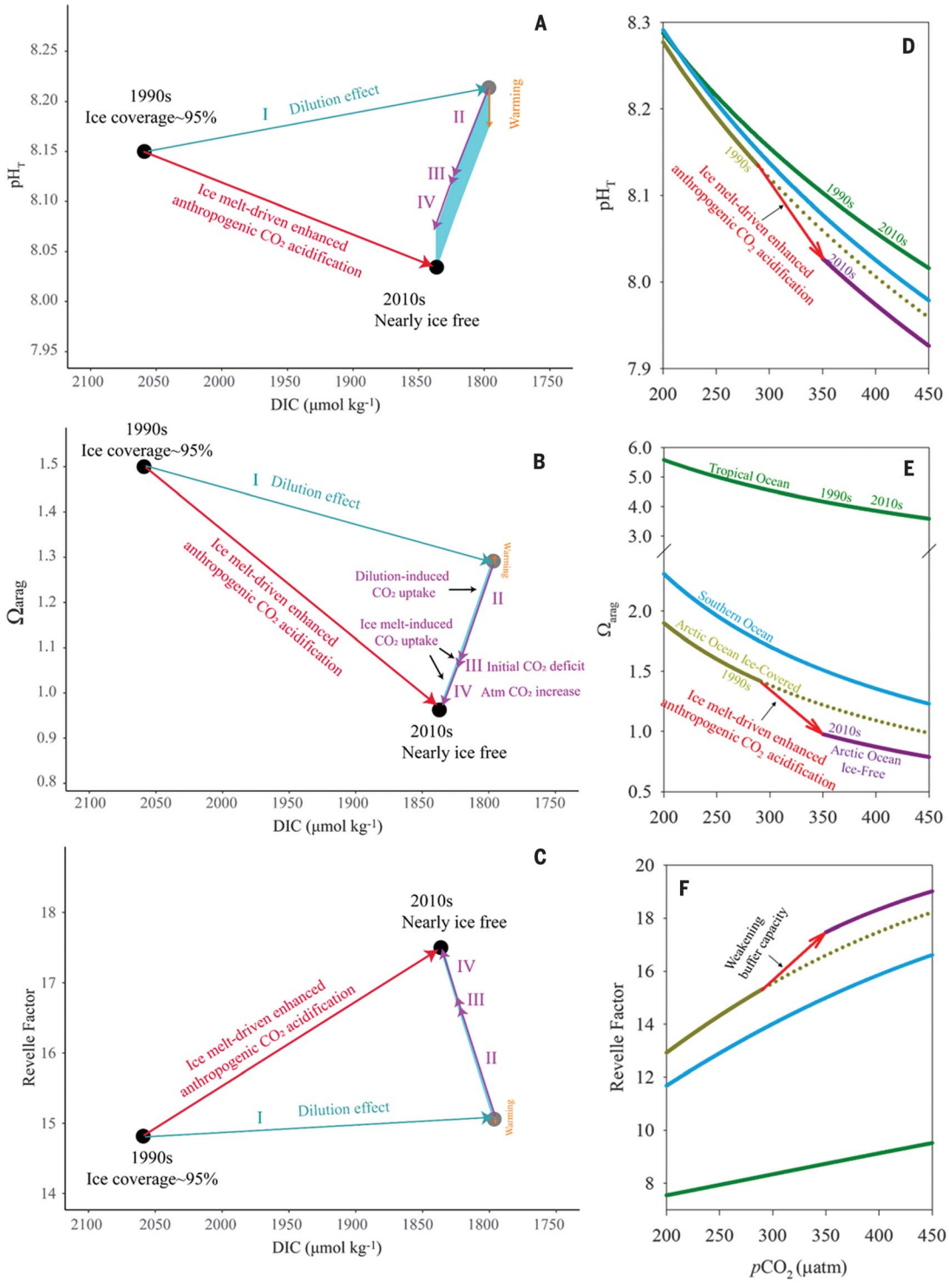

Fig. 4. Sea ice loss and melt are amplifying surface ocean acidification in the Arctic Ocean basin. (**A** to **C**) The decadal progression of ocean acidification with respect to pH_T (A), Ω_{arag} (B), and the Revelle factor (C). The black dots represent the observational conditions for pH_T, Ω_{arag}, and the Revelle factor (values calculated from decadal means; table S3). The gray dot represents the initial condition after sea ice melt [a two-endmember mixing model consisting of 1990s ice-covered seawater and ice-melt water was applied to calculate diluted TA and DIC and carbonate parameters; TA was used as a tracer, and the meltwater endmember was obtained from (*40*)]. The arrows indicate the processes of warming (orange), dilution (I, dark cyan), dilution-induced CO_2 uptake (II, magenta), and ice melt–induced CO_2 uptake (III and IV, magenta). The dilution-induced process (II) refers to the uptake of CO_2 to compensate for the dilution-lowered Pco_2 (increased up to the initial Pco_2 in the 1990s; fig. S15); the ice melt–induced process refers to the following CO_2 uptake from the atmosphere, where initial CO_2 deficit term (III) denotes the disequilibrium between 1990s Pco_2 and air Pco_2, and atmospheric (Atm) CO_2 increase term (IV) denotes acidification driven by the air Pco_2 increase from the 1990s to 2010s. The blue-shaded areas indicate the possible decadal variations in pH_T, Ω_{arag}, and the Revelle factor, which were synergistically affected by warming and CO_2 uptake. The initial status of the ice-covered Canada Basin in the 1990s is set as salinity (S) = 31.3, temperature (T) = −1.6°C, TA = 2192 μmol kg^{-1}, DIC = 2059 μmol kg^{-1}, and Pco_2 = 278 μatm (table S3). Dilution with a meltwater endmember of TA ≈ 70 μmol kg^{-1} (*40*) results in a lower TA of 1912 μmol kg^{-1}, DIC of 1792 μmol kg^{-1}, and Pco_2 of 214 μatm (and simultaneously lower Ω_{arag} owing to decreased salinity and carbonate ion concentration, but higher pH_T owing to decreased hydrogen ion concentration) (dilution effect I). When Pco_2 increases back to the initial Pco_2 level before ice melting in the 1990s (dilution-induced CO_2 uptake, II), it causes a decrease in pH_T of 0.10 and a decrease in Ω_{arag} of 0.25. These decreases will be driven by subsequent ice melt–induced CO_2 uptake (III and IV, where IV represents the air Pco_2 decadal increase of 38 μatm and corresponding changes in pH_T and Ω_{arag}), which leads to a further decrease in pH_T of 0.05 and a decrease in Ω_{arag} of 0.11. (**D** to **F**) Surface-water acidification parameters as a function of surface Pco_2 for the global tropical ocean, the Southern Ocean, and the Arctic Ocean (ice-covered and ice-free scenarios) from the multidecadal perspective. The dashed lines are linear extensions of the trendlines, which may not be realistic. Calculations were made using CO2SYS with the following input values: T = 26°C, S = 35, and TA = 2332 μmol kg^{-1} for the tropical ocean; T = −0.3°C, S = 34, and TA = 2297 μmol kg^{-1} for the Southern Ocean; T = −1.6°C, S = 31, and TA = 2192 for the Arctic Ocean, ice-covered scenario; and T = 0.72°C, S = 26, and TA = 1912 μmol kg^{-1} for the Arctic Ocean, ice-free scenario (table S3). The red arrows refer to the processes that regulate decadal changes in pH_T, Ω_{arag}, and the Revelle factor in (A) to (C).

earlier 18-year period (1994 to 2012) has the steepest decline trends in pH_T (−0.0098 ± 0.0019 $year^{-1}$) and Ω_{arag} (−0.0342 ± 0.0077 $year^{-1}$), which corresponds well with the steepest decrease in sea ice (Fig. 2). However, the decreasing trends of both pH_T and Ω_{arag} were slower during 2010 to 2020, which is consistent with the alleviated reduction of sea ice since 2008, though a strong interannual variability is apparent (Fig. 2A). Nevertheless, even during this period, the rate of pH_T decrease is still comparable to rates of other ocean basins (Fig. 2A and table S2), which are mainly driven by the increasing atmospheric CO_2. Unlike pH_T, no statistically significant trend for Ω_{arag} was found during 2010 to 2020, reflecting the counteracting effect of warming. Clearly, massive sea ice retreat, modulated by the large-scale climate change pattern, has played a critical role in the fast acidification in the Arctic Ocean over the past two to three decades.

To explain the link between rapid long-term pH_T and Ω_{arag} decline rates and the massive sea ice loss in the Arctic Ocean, a thorough understanding of the evolution of carbonate chemistry in response to the sea ice condition is required. In the 1990s, when most of the Arctic Ocean surface was covered by sea ice, the transfer of CO_2 from the atmosphere into the surface waters was impeded by sea ice (fig. S1A), resulting in a large deficit of DIC from the atmospheric equilibrium value (ΔDIC = −25 μmol kg^{-1}; figs. S13C and S14). As a consequence, the cold surface seawater beneath the sea ice has a high potential to absorb atmospheric CO_2 once it is exposed to the atmosphere.

Since the 2000s, the Arctic Ocean has experienced accelerated warming and substantial sea ice retreat (e.g., ice extent was at its lowest in the summer of 2012) (Fig. 2A and fig. S1B). We used a simple one-dimensional (1D) dynamic model to simulate the response of P_{CO_2}, pH, and Ω_{arag} to the decrease of sea ice (Fig. 3; see supplementary materials for a description of the model). We found that, under partially or newly ice-free conditions, the low-P_{CO_2} waters that were originally under the ice were exposed to higher atmospheric P_{CO_2} and rapidly took up CO_2 through air-sea gas exchange (Fig. 3D). In other words, the initial CO_2 deficit resulted in a CO_2 increase "boost" over that time period. The shallow surface mixed layer and strong stratification (*34*, *35*) also prevented the dilution of the absorbed CO_2, leading to rapid responses of the carbonate system parameters (Fig. 3, B and C, and fig. S1B).

The rapid decreases in pH_T and Ω_{arag} along with sea ice retreat are seen not only over a seasonal time scale but also over a decadal time scale (Fig. 3). We further quantified and decomposed the decadal drivers of acidification (table S7) and translated the results to a graphic illustration (Fig. 4, A to C). We found that the net increase in DIC due to CO_2 uptake plays the predominant role in regulating acidification, with minor contributions from warming and dilution. However, we further diagnosed that, indirectly, approximately half of the changes in P_{CO_2}, pH_T, and Ω_{arag} that resulted from CO_2 uptake are attributable to the additional CO_2 deficit triggered by sea ice melt (i.e., dilution of TA and DIC leads to lower initial P_{CO_2}; see Fig. 4, A to C, fig. S15, and table S7). Thus, the indirect effect of dilution on the seawater carbonate system through the promotion of CO_2 uptake is an important factor driving acidification and weakening buffer capacity in the western Arctic Ocean (Fig. 4, A to C).

The progression in sea ice loss represents a major change in seawater carbonate chemistry, from a state of well-buffered seawater with relatively high alkalinity and low P_{CO_2} underneath the sea ice (fig. S1A) to a meltwater-diluted state characterized by lower alkalinity, higher P_{CO_2}, and lower buffer capacity under the partially or fully ice-free surface (Fig. 4, D to F, and fig. S1C). As a result, atmospheric CO_2 invasion would lead to a greater overall decrease in pH_T, Ω_{arag}, and buffer capacity in seawater diluted by meltwater than the original water (Fig. 4, A to C, and fig. S15), illustrated also as a jump from one pH_T-P_{CO_2} evolving locus along the high iso-alkalinity line in the 1990s to the low iso-alkalinity line in the 2010s (Fig. 4, D to F). We name this distinctive mechanism "ice melt–driven enhanced anthropogenic CO_2 acidification." The mechanism explains the amplified rapid acidification observed in the Arctic Ocean over the past two to three decades, in contrast to the slower acidification in other global oceans along only one alkalinity line (Fig. 4, D to F). This mechanism could conceivably also operate in the sea ice zone within the Southern Ocean, where seasonal sea ice melt also plays an important role in sea surface CO_2 dynamics and in air-sea CO_2 gas exchange (*36*).

We must also point out that further warming could result in contrasting impacts on pH_T and Ω_{arag} trends (fig. S16; see supplementary text for details). This phenomenon has emerged in late summer in ice-free southern regions since the 2010s, where both warming and CO_2 uptake from the atmosphere decreased pH_T (fig. S16A), whereas warming (when it exceeds +1°C) increased and CO_2 uptake decreased Ω_{arag} (fig. S16B). When temperature further increases, the net Ω_{arag} trend could even be positive, similar to what has been observed in some other parts of the world's oceans (*37*, *38*); this is also illustrated as the cancellation effect of the red-plus circle by the blue-minus circle in Fig. 1L).

Although Arctic sea ice coverage has fluctuated over the past decade, it is also shifting from multiyear ice to first-year ice (fig. S17). This thinning trend of sea ice implies that summer sea ice will continue to decline in extent and lower the seawater alkalinity and buffer capacity until the Arctic Ocean is turned into an ice-free region. Finally, although the overall freshwater increase, including that from rivers, has decreased the anthropogenic CO_2 inventory in the subsurface water (*19*), there is, at present, no significant decadal trend in river-water content in the surface layer (Fig. 2B). Therefore, both larger winter-to-summer meltwater-induced seawater alkalinity dilution and greater subsequent CO_2 uptake from the atmosphere are expected to be the dominant processes in surface waters. As a consequence, the "ice melt–driven enhanced anthropogenic CO_2 acidification" mechanism may continue to operate over the next few decades, becoming even more pronounced until the time that sea ice completely disappears during summer (at which time, Arctic Ocean surface seawater may reach its lowest alkalinity) (Fig. 4). Therefore, this greatly amplified summertime ocean acidification modulated by large-scale climate change may lead to long-lasting impacts on the biogeochemistry, ecosystem, and organisms in the Arctic Ocean basins.

REFERENCES AND NOTES

1. J. C. Orr *et al*., *Nature* **437**, 681–686 (2005).
2. N. R. Bates *et al*., *Oceanography* **27**, 126–141 (2014).
3. T. Takahashi *et al*., *Mar. Chem.* **164**, 95–125 (2014).
4. L. Kwiatkowski, J. C. Orr, *Nat. Clim. Change* **8**, 141–145 (2018).
5. N. Gruber *et al*., *Science* **337**, 220–223 (2012).
6. M. Steinacher, F. Joos, T. Frolicher, G.-K. Plattner, S. C. Doney, *Biogeosciences* **6**, 515–533 (2009).
7. L. Bopp *et al*., *Biogeosciences* **10**, 6225–6245 (2013).
8. A. Yamamoto, M. Kawamiya, A. Ishida, Y. Yamanaka, S. Watanabe, *Biogeosciences* **9**, 2365–2375 (2012).
9. J. A. Screen, I. Simmonds, *Nature* **464**, 1334–1337 (2010).
10. A. Proshutinsky, D. Dukhovskoy, M. L. Timmermans, R. Krishfield, J. L. Bamber, *Philos. Trans. R. Soc. London Ser. A* **373**, 20140160 (2015).
11. K. A. Giles, S. W. Laxon, A. L. Ridout, D. J. Wingham, S. Bacon, *Nat. Geosci.* **5**, 194–197 (2012).
12. R. A. Woodgate, T. J. Weingartner, R. Lindsay, *Geophys. Res. Lett.* **39**, 2012GL054092 (2012).
13. K. M. Lewis, G. L. van Dijken, K. R. Arrigo, *Science* **369**, 198–202 (2020).
14. J. R. Farmer *et al*., *Nat. Geosci.* **14**, 684–689 (2021).
15. W. J. Cai *et al*., *Science* **329**, 556–559 (2010).
16. Z. Ouyang *et al*., *Nat. Clim. Change* **10**, 678–684 (2020).
17. F. A. McLaughlin, E. C. Carmack, *Geophys. Res. Lett.* **37**, L24602 (2010).
18. Y. Zhuang *et al*., *Environ. Res. Lett.* **16**, 054047 (2021).
19. R. J. Woosley, F. J. Millero, *Limnol. Oceanogr.* **65**, 1834–1846 (2020).
20. M. Yamamoto-Kawai, F. A. McLaughlin, E. C. Carmack, S. Nishino, K. Shimada, *Science* **326**, 1098–1100 (2009).
21. D. Qi *et al*., *Nat. Clim. Change* **7**, 195–199 (2017).
22. L. L. Robbins *et al*., *PLOS ONE* **8**, e73796 (2013).
23. J. N. Cross, J. T. Mathis, R. S. Pickart, N. R. Bates, *Deep Sea Res. Part II Top. Stud. Oceanogr.* **152**, 67–81 (2018).
24. I. Semiletov *et al*., *Nat. Geosci.* **9**, 361–365 (2016).
25. J. T. Mathis *et al*., *Geophys. Res. Lett.* **39**, L07606 (2012).
26. Y. Zhang, M. Yamamoto-Kawai, W. J. Williams, *Geophys. Res. Lett.* **47**, e60119 (2020).
27. J. G. Wynn, L. L. Robbins, L. G. Anderson, *J. Geophys. Res. Oceans* **121**, 8248–8267 (2016).

28. Y. Luo, B. P. Boudreau, A. Mucci, *Nat. Commun.* **7**, 12821 (2016).
29. J. Terhaar, L. Kwiatkowski, L. Bopp, *Nature* **582**, 379–383 (2020).
30. V. J. Fabry, J. B. McClintock, J. T. Mathis, J. M. Grebmeier, *Oceanography* **22**, 160–171 (2009).
31. J. C. Orr, J. M. Epitalon, A. G. Dickson, J. P. Gattuso, *Mar. Chem.* **207**, 84–107 (2018).
32. L. Gregor, N. Gruber, *Earth Syst. Sci. Data* **13**, 777–808 (2021).
33. Tu, Z. *et al*., *Geophys. Res. Lett.* **48**, e2021GL093844 (2021).
34. C. Peralta-Ferriz, R. A. Woodgate, *Prog. Oceanogr.* **134**, 19–53 (2015).
35. E. C. Fine, S. T. Cole, *J. Geophys. Res. Oceans* **127**, e2021JC018056 (2022).
36. M. S. Brown *et al*., *Nat. Clim. Change* **9**, 678–683 (2019).
37. W. J. Cai *et al*., *Nat. Commun.* **11**, 2691 (2020).
38. Y. Wu *et al*., *Geophys. Res. Lett.* **48**, e2021GL094473 (2021).
39. B. Huang *et al*., *J. Clim.* **34**, 2923–2939 (2020).
40. A. Mo *et al*., *Front. Mar. Sci.* **9**, 766810 (2022).

ACKNOWLEDGMENTS

We thank the many contributors to the CHINARE, SOCAT, OCADS, LDEO, R/V Mirai cruises (JAMSTEC), and WHOI datasets as well as the many research vessels and crews that contributed to the collection of data used in this study. This is Pacific Marine Environmental Laboratory (PMEL) contribution number 5115. We thank H. Sun, Z. Gao, T. Li, A. Collins, and Y. Zhang for data collection and L. Yuan, X. Chen, D. Gui, Z. Feng, and J. Zhao for data processing. We also thank T. Clayton for improving the language. We are also grateful to the three anonymous reviewers. **Funding:** This work was supported by the National Key Research and Development Program of China (2019YFE0114800); the National Natural Science Foundation of China (41941013, 42176230, 41630969, and 42188102); the Ocean Negative Carbon Emissions (ONCE) Program, Key Deployment Project of Centre for Ocean Mega-Research of Science; Chinese Academy of Sciences (CAS) (grant no. COMS2020Q12); Chinese Projects for Investigations and Assessments of the Arctic and Antarctic (CHINARE2017-2020); and the Natural Science Foundation of Fujian Province, China (2019Jo5148). The University of Delaware group has been supported by the National Science Foundation (NSF) (ARC-0909330, PLR-1304337, and OPP-1926158) and the National Oceanic and Atmospheric Administration (NOAA) (NA09OAR4310078). R.A.F. was supported by the NOAA Ocean Acidification Program and the Pacific Marine Environmental Laboratory. **Author contributions:** L.C., D.Q., and W.-J.C. designed the program, and D.Q. and Z.O. executed the fieldwork. D.Q., Y.W., Z.O., and W.-J.C. analyzed the data and prepared the paper. All authors contributed to discussion and writing of the manuscript. **Competing interests:** The authors declare that they have no competing interests. **Data and materials availability:** The CHINARE surface Pco_2 datasets are deposited in SOCAT (with 2008, 2010, 2012, 2014, 2016, and 2018 already archived in SOCATv2021 and 2017 and 2020 to be archived in SOCATv2023). These datasets are also accessible via the Ocean Carbon and Acidification Data System (OCADS) (https://www.ncei.noaa.gov/access/ocean-carbon-acidification-data-system/oceans/VOS_Program/Xuelong.html). The CHINARE bottle data have been submitted to the Global Ocean Data Analysis Project (GLODAP) and will be archived in v2023 as well. In addition, the integrated Pco_2 dataset used in this study is deposited in Mendeley Data (https://data.mendeley.com/datasets/2ccwgyf6cw/1).

SUPPLEMENTARY MATERIALS

science.org/doi/10.1126/science.abo0383
Materials and Methods
Supplementary Text
Figs. S1 to S20
Tables S1 to S7
References (*41*–*73*)

Submitted 9 January 2022; accepted 6 September 2022
10.1126/science.abo0383

Climate change drives rapid decadal acidification in the Arctic Ocean from 1994 to 2020

Di Qi, Zhangxian Ouyang, Liqi Chen, Yingxu Wu, Ruibo Lei, Baoshan Chen, Richard A. Feely, Leif G. Anderson, Wenli Zhong, Hongmei Lin, Alexander Polukhin, Yixing Zhang, Yongli Zhang, Haibo Bi, Xinyu Lin, Yiming Luo, Yanpei Zhuang, Jianfeng He, Jianfang Chen, and Wei-Jun Cai

Science **377** (6614), . DOI: 10.1126/science.abo0383

Acceleration in the Arctic

The Arctic is warming at a rate faster than any comparable region on Earth, with a consequently rapid loss of sea ice there. Qi *et al*. found that this sea ice loss is causing more uptake of atmospheric carbon dioxide by surface water and driving rapid acidification of the western Arctic Ocean, at a rate three to four times higher than that of the other ocean basins. They attribute this finding to melt-driven addition of freshwater and the resulting changes in seawater chemistry. —HJS